https://doi.org/10.1590/jatm.v13.1239 ORIGINAL PAPER

Inductive Coupling Discharge Characteristics of a 10-cm Dual-Stage 4-Grid Radiofrequency Ion Thruster

Yanxu Pu[1], Wenshuang Zhang[2], Xingda Li[1,*], Lianjun Jia[1], Xinfeng Sun[1], Chenchen Wu[1], Xianzhong Liu[1], Xian Wu[1]

1.China Academy of Space Technology – Lanzhou Institute of Physics –Science and Technology on Vacuum Technology and Physics Laboratory– Lanzhou/Ganshu – China. 2.China Academy of Space Technology – Institute of Telecommunication and Navigation Satellites – Beijing – China.

*Correspondence author: tjulxd@126.com

ABSTRACT

In this study, the numerical simulations are used to simulate the discharge process of a 10-cm dual-stage 4-grid (DS4G) radiofrequency (RF) ion thruster, and the effects of RF coil turns, and electrical parameters on the key plasma parameters inside the discharge chamber are investigated. Thus, the optimal design parameters of the thruster are obtained. The RF plasma source has high inductive coupling discharge efficiency when the number of coil turns is six and the operational frequency is 2 MHz. The simulation results show that increasing the number of coil turns can effectively increase the plasma density inside the discharge chamber, and thus improve the efficiency of the inductive coupling discharge, and the operational frequency affects the characteristics of the inductively coupled discharge by influencing the depth of the plasma skinning layer. An experimental thruster demonstrated the 10-cm DS4G RF ion thruster can achieve super high specific impulse. The correctness of the simulation model is verified by the experiment results of the thruster, which will be useful for the optimal design of radio ion thruster or ion sources.

Keywords: RF ion thruster; Performance; Plasma; Fluid physical.

INTRODUCTION

Compared with chemical propulsion, ion electric propulsion has significant advantages, such as small thrust, high specific impulse, long life, and continuous thrust regulation, which can save the propellant and increase the load ratio for spacecraft (Goebel 2008; Mazouffre 2016). Therefore, ion electric propulsion has been successfully applied to space missions, such as spacecraft position maintenance, orbit transfer, and deep space exploration.

Received: Apr. 01, 2021 | **Accepted:** Oct. 20, 2021
Peer Review History: Single Blind Peer Review.
Section editor: José Atílio Fritz Fidel Rocco

The radiofrequency (RF) ion thruster uses inductive coupling discharge to produce plasma. Because the thruster has no main discharge cathode, the thruster has the characteristics of high efficiency, long life, simple structure, easy to integrate. Given their wide application and development prospect, RF ion thrusters have received extensive interest (Goebel 2008). The transformer model for inductively coupled discharges was proposed by Piejak *et al.* (1992), El-Fayoumi and Jones (1998), Keller *et al.* (1993). In this model, the coil and the plasma form a transformer, where the plasma is equated to a single-turn hollow secondary coil. Chabert *et al.* (2012) introduced the transformer model to calculate the key plasma parameters of the discharge chamber and calculate the performance indexes of the RF ion thruster. Tsay *et al.* (2008) from the Massachusetts Institute of Technology and Emre of Turkey conducted a numerical simulation of the RF ion thruster discharge chamber according to a two-dimensional fluid model. Henrich and Heiliger (2013) of the Giessen University in Germany established a comprehensive evaluation model to investigate the influence of various input parameters on thruster. Rakhimov from the Skolkovo Institute of Science and Technology and Milov from Avant-Space Systems LLC of Skolkovo Innovation Center introduced a scheme for a complex calculation of the parameters of a RF ion thruster (Rakhimov *et al.* 2019). Based on this scheme, the ion optical system, RF power loss, plasma parameters distribution, heat flux, and temperature fields are analyzed. According to the numerical results, the operation mode and efficiency of the thruster were optimized, and the verification experiment was carried out. Lucken *et al.* (2019) developed a global modeling of the RF ion thruster by using theories of instability enhanced plasma transport. The unstable xenon plasma is simulated using a 2D particle-in-cell (PIC) simulation. Pham and Shin (2020) have improved the zero-dimensional analytical model by incorporating most physical phenomena expected in RF ion thruster, such as secondary electron emission, double ionization, a variable Clausing factor (related to molecular flux and total incoming flux), grid optical transparency, and an ion confinement factor affected by the electromagnetic field. The research shows that the ion confinement factor is the key factor affecting the inductive coupling discharge characteristics. In summary, researchers usually use a combination of numerical simulation and experimental verification to optimize the RF discharge chamber to improve the efficiency of inductive coupling discharge.

In terms of product development, only the European space agency and Australia jointly developed a prototype of a dual-stage four-grid (DS4G) ion thruster with a RF source in 2006 (Bramanti *et al.* 2006). The experimental result suggested that the DS4G structure can effectively improve the specific impulse (14,000–15,000 s), thrust and power density (8.4 $mN \cdot cm^{-2}$, 740 $W \cdot cm^{-2}$) of the thruster. High total efficiency (70%) and high propellant utilization efficiency (96%) can be achieved by using RF plasma source. However, the active diameter of grid was 2 cm, 4-grid system consisting of 43 apertures of 1-mm diameter. This thruster is a low-power laboratory prototype, which is a certain distance from engineering applications.

This paper is aimed at design a 10-cm DS4G RF ion thruster with engineering application value according to the results of numerical calculation. Meanwhile, the influence of design parameters on the key plasma parameters in the discharge chamber is studied, which provides a theoretical basis for the subsequent performance optimization of the thruster.

RADIOFREQUENCY THRUSTER

The RF ion thruster generates plasma through inductive coupling discharge. As shown in Fig. 1, it plots the schematic of RF ion thruster. When the RF absorbed power and the dissipated power reach a balance, a continuous and stable RF inductive coupling discharge is formed. Its working principle is that the ions of discharge plasma are focused, accelerated, and extracted by a grids system with positive and negative bias voltage, respectively. Then, the thrust is forced by the high-speed ions, while the electrons are absorbed by the positive bias grid. The extraction high speed charged ions are neutralized by electrons generated by the neutralizer, so as to maintain the electrical neutrality of the system.

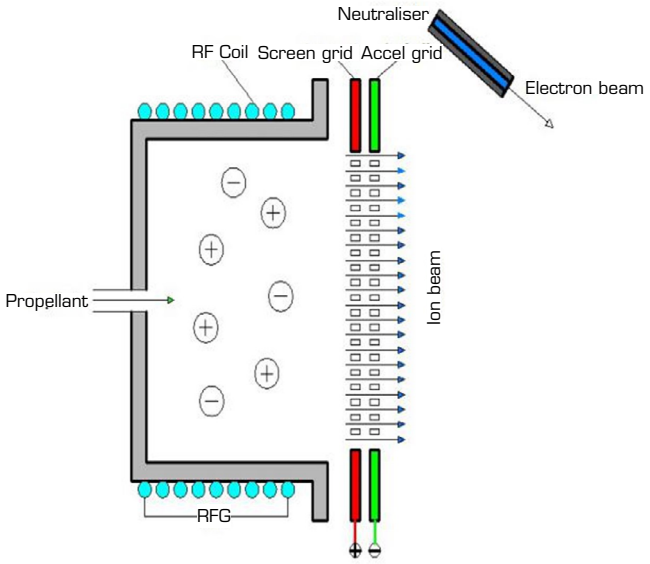

Figure 1. Schematic diagram of RF ion thruster.

INDUCTIVE COUPLING DISCHARGE PLASMA MODELS

The inductive coupled discharge model consists of three main components: electromagnetic, transformer, and fluid models. The electromagnetic model couples the coil with the plasma by solving for the magnetic vector potential, and the solved electric and magnetic fields are added to the momentum equations of the fluid model. The transformer model solves for the equivalent circuit parameters, which are used as the basis to obtain the coil currents by depositing power and adding the coil currents to the electromagnetic model. The fluid model solves for the plasma-related parameters via the continuity equation.

The electric and magnetic fields calculated from the electromagnetic model are coupled in the fluid equations, which contain the particle number conservation equation, the momentum conservation, electron energy balance, and potential equations for the three particles: electrons, ions, and neutral atoms. The following are assumed: the density of the ions in the calculation region is equal to the density of the electrons; the ions and the neutral atoms are moving much less rapidly than the electrons; and the electrons are in approximate drift-diffusion motion.

The particle number conservation equations are as follows:

$$\frac{\partial n_i}{\partial t} + \nabla \cdot (n_i v_i) = \dot{R}_\iota \tag{1}$$

$$\frac{\partial n_e}{\partial t} + \nabla \cdot (n_e v_e) = \dot{R}_e \tag{2}$$

$$\frac{\partial n_n}{\partial_\iota} + \nabla \cdot (n_n v_n) = -\dot{R}_n \tag{3}$$

The first term on the left-hand side of the Eqs. 1–3 describes the change in the particle number density at a particular point in space, the second term on the left-hand side of the Eqs. 1–3 describes the change in the particle number density caused by the flow of particles into or out of the calculation region, and the right-hand side of the Eqs. 1–3 represents the particle production rate.

The conservation of momentum equations are as follows:

$$m_i n_i \left(\frac{\partial v_i}{\partial t} + v_i \cdot \nabla v_i\right) + k\nabla(n_i T_i) = e n_i E + e n_i v_i \times B - m_i n_i \upsilon_{in}(v_i - v_n) - m_i n_i \upsilon_{in}(v_i - v_e) \tag{4}$$

$$m_e n_e \left(\frac{\partial v_e}{\partial t} + \mathrm{v}_e \cdot \nabla v_e\right) + k\nabla(n_e T_e) = e n_e E + e n_e v_e \times B - m_e n_e \upsilon_{en}(v_e - v_n) - m_e n_e \upsilon_{en}(v_e - v_i) \quad (5)$$

$$m_n n_n \left(\frac{\partial v_n}{\partial t} + \mathrm{v}_n \cdot \nabla v_n\right) + k\nabla(n_n T_n) = -m_n n_n \upsilon_{in}(v_n - v_i) - m_n n_n \upsilon_{in}(v_n - v_e) \quad (6)$$

The first term on the left side of the Eqs. 4–6 represents the acceleration and inertia terms, the second term on the left side of the Eqs. 4–6 represents the pressure gradient force, and the right side of the Eqs. 4–6 represents the electric field, magnetic field, and friction forces, respectively. The momentum equation contains three equations for the three particles, each containing three components in the axial, radial, and angular directions for a total of nine equations.

The electron energy balance equations are as follows:

$$\frac{3}{2}\frac{\partial}{\partial t}(n_e e T_e) = P_{abs} - P_{coll} - P_{wall} \quad (7)$$

$$P_{abs} = \sigma |E|^2 \quad (8)$$

$$P_{coll} = n_e n_n e \langle v_e \sigma_i \rangle U_{ion} + n_e n_n e \langle v_e \sigma_{exc} \rangle U_{exc} \quad (9)$$

$$P_{wall} = (2eT_e + e\emptyset_{sheath})\Gamma_e \quad (10)$$

The left-hand side of the Eqs. 7–10 represents the change in electron energy in the calculated region, while the right-hand side of the Eqs. 7–10 represents the absorbed electron power, the collisional loss power, including ionization and excitation, and the wall energy loss, respectively.

The fluid model is, therefore, solved for seven equations, which involve solving for seven parameters: electron density n_e, ion density n_i, neutral density n_n, ion velocity v_i, electron velocity v_e, neutral velocity v_n, and electron temperature T_e.

R_i, R_e, and R_n are the ion, electron, and neutral atom production rates, respectively; ν_{in}, ν_{ei}, and ν_{en} are the ion-neutral atom, electron-ion, and electron-neutral atom collision frequencies, respectively. k is the Boltzmann constant; e is the meta-charge power; T_i, T_e, and T_n are the ion, electron, and neutral temperatures, respectively. Γ_e is the electron flux, P_{abs} is the power deposited into the plasma, P_{coll} is the collisional power loss, and P_{coll} is the energy loss of the electrons flowing to the wall.

The calculation area is divided into a grid, as shown in Fig. 2. The boundary layer mesh near the walls of the discharge chamber is divided to accurately describe the state of space charge separation between the electrons and the ions near the walls. A fine mesh is added to the coil domain for solution due to the presence of metal skin effects.

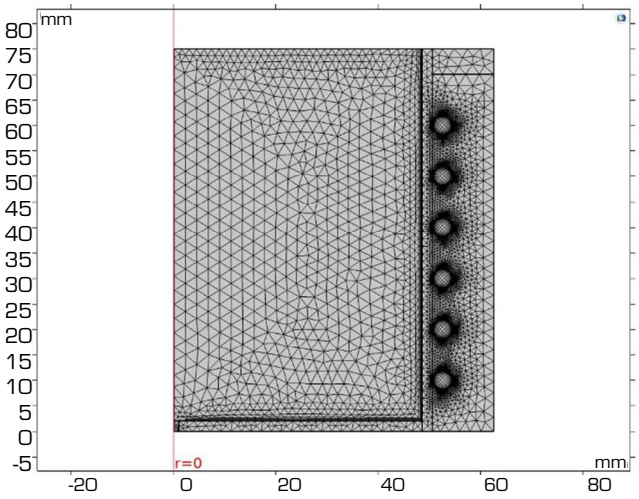

Figure 2. Calculation area meshing.

Solving for the sheath region requires reducing the grid to the Debye length order of magnitude, which requires a considerably long computational time. Therefore, the computational region only extends to the pre-sheath region, imposing pre-sheath boundary conditions at the wall and without solving for the sheath, that is, ions flow towards the wall at Bohm velocity, reach the wall and compound with electrons as neutral atoms, and return to the discharge region. The flux of ions leaving the computational region is equal to the flux of neutral atoms entering the computational region, and the wall has zero potential relative to the plasma.

SIMULATION RESULTS

The simulation modelling of the inductive coupled discharge characteristics is performed using the COMSOL Multiphysics software. The initial conditions for the discharge are as follows: the electron density is 1×10^{15} m^{-3}, the temperature is 300 K, the initial average electron energy is 5 eV, and the electron mobility is 4.0×10^{24} m^2/(V·s). The plasma has an excitation to stable discharge process, and the simulation time for this model is set to 0.001 s, which is sufficient to establish a stable plasma discharge. The results below are all calculated at 0.001 s.

Input parameters discharge chamber pressure, gas type, operational frequency, coil turns, and RF power are 2.66 Pa, xenon, 2 MHz, six, and 120 W, respectively. The distribution of the key plasma parameters, such as electron density, electron temperature, plasma potential, the magnetic field generated by the RF coil, and the power deposition inside the discharge chamber, are calculated, and the results are shown in Fig. 3.

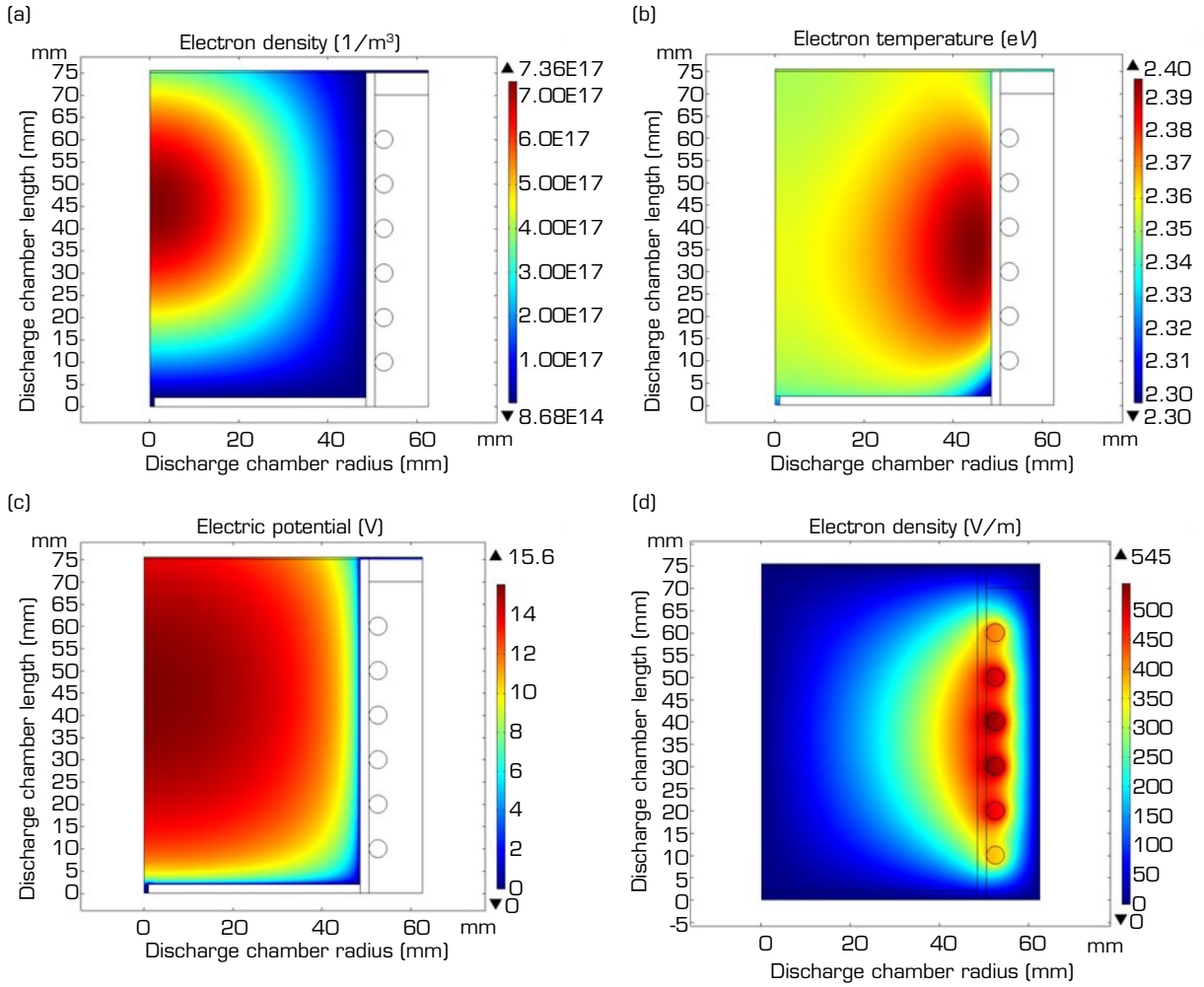

Figure 3. Distribution of key plasma parameters. (a) Electron density distribution; (b) Electron temperature distribution; (c) Electric potential distribution; (d) Electric field distribution; (e) Total power dissipation density distribution.

Figure 3a shows the electron density distribution, with the highest electron density in the middle region of the discharge chamber and the lowest near the walls, which is mainly due to the two-stage diffusion effect; Fig. 3b shows the electron temperature distribution, which is the highest near the wall of the discharge chamber as the electrons gain energy mainly in the skinning layer near the wall (Takahashi *et al.* 2017); Fig. 3c is the potential distribution, which obeys the Boltzmann relationship, like the electron density distribution; Fig. 3d is the distribution of the electric field generated by the coil, with the coil in the middle producing the largest electric field; Fig. 3e is the power deposition density distribution. The range of power density deposition is the skinning layer region, where the particles gain energy and the depth of the skinning layer depends mainly on the RF power frequency, collision frequency.

EFFECT OF RF COIL TURNS ON DISCHARGE PLASMA

Changes in the number of RF coil turns cause changes in the electron density, electric field, and electron temperature inside the discharge chamber, which affect the discharge efficiency of the inductive coupling. To improve the efficiency of the inductive coupled discharge and optimize the thruster design, the variation law of the plasma parameters inside the discharge chamber was determined using the controlled variable method, varying the number of coil turns as shown in Figs. 4–6.

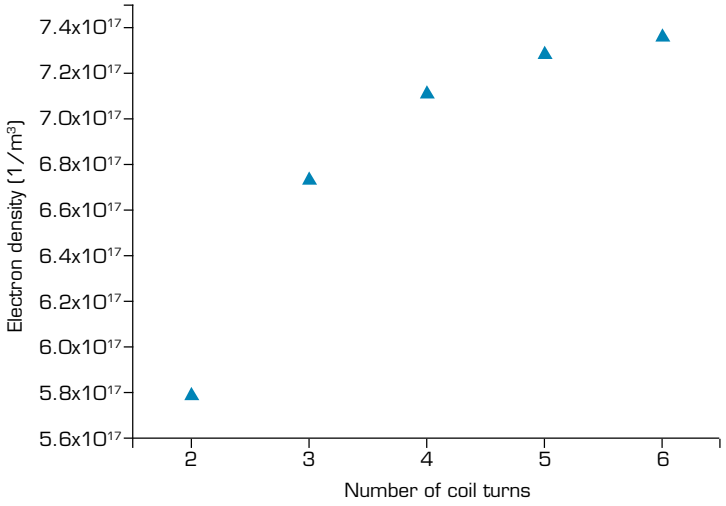

Figure 4. Electron density vs. number of coil turns at the axis of the discharge chamber.

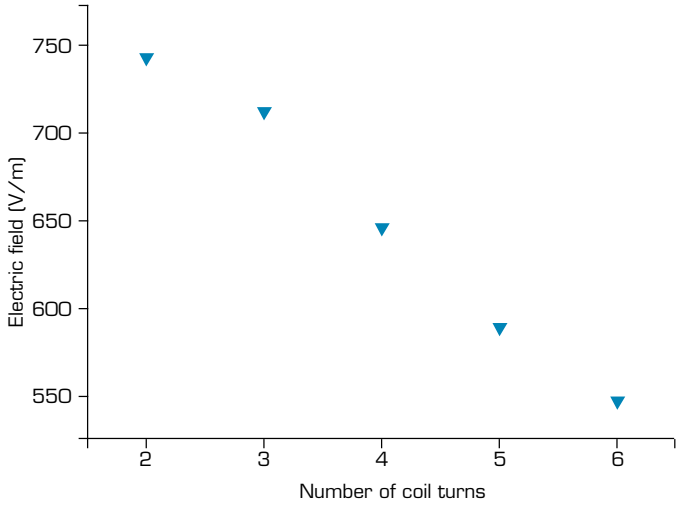

Figure 5. Maximum electric field generated by the coil vs. number of coil turns.

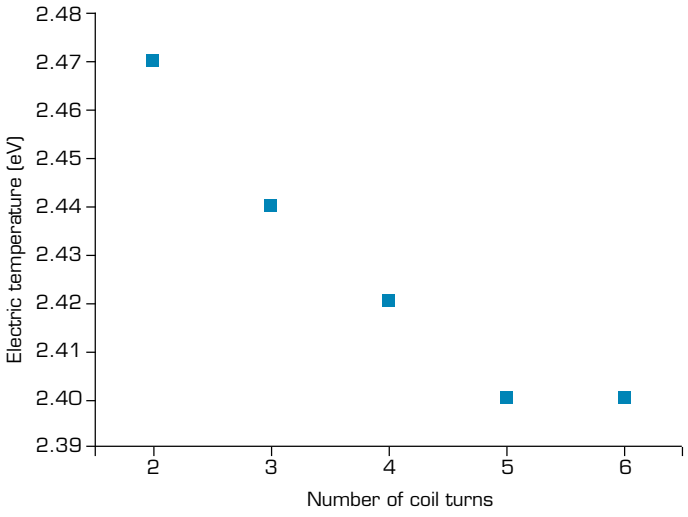

Figure 6. Maximum electron temperature inside the discharge chamber vs. number of coil turns.

Figure 4 shows the variation of electron density at the axis with the number of coil turns. The electron density increases with the number of coil turns, from 5.78×10^{17} to 7.36×10^{17} m^{-3}. Figure 5 shows the variation of the maximum electric field value generated by the coil with the number of coil turns. The maximum electric field value generated by the coil decreases with the increase in the number of coils, from 745 to 545 $V \cdot m^{-1}$. Figure 6 shows the variation of the electron temperature inside the discharge chamber with the number of coil turns, that is, the electron temperature decreases slightly in the 2.47–2.40 eV range with the increase in the number of coil turns. Increasing the number of coil turns can effectively increase the plasma density inside the discharge chamber, reduce the electric field generated by the coil, reduce energy dissipation, and thus improve the efficiency of the inductive coupling discharge. For the RF ion thruster in this study, the plasma density inside the discharge chamber is high and the energy loss is low when the number of RF coil turns is 6.

EFFECT OF RF ELECTRICAL PARAMETERS ON DISCHARGE PLASMA

The main RF parameters affecting the inductive coupled discharge characteristics are the operational frequency and RF power. Compare the variation of the plasma density inside the discharge chamber with the number of turns of the coil under different radio frequencies, as shown in Fig. 7. It can be seen that the electron density increases with the number of turns of the coil at the two frequencies. Comparing the electron density at different frequencies under the same number of coil turns, it can be seen that the electron density at 2 MHz is significantly greater than at 13.56 MHz. Therefore, for the discharge chamber studied in this paper, when the RF power frequency is 2 MHz and the number of coil turns is six, there is a higher discharge efficiency.

Figure 8a shows the variation of the electron density with the RF power at the axis of the discharge chamber with different RF power frequency. The figure indicates that the electron density has an obvious positive relationship with the RF power. The comparison of electron density at the same power and different frequencies indicates that the electron density at 2 MHz is greater than that at 13.56 MHz. This result is mainly because the plasma skinning depth at 2 MHz is approximately 1/2 (Fig. 3e) of the radius of the discharge chamber, resulting in higher RF power coupling efficiency, whereas at 13.56 MHz the skinning depth is much smaller than the radius of the discharge chamber, resulting in more charged particles compounding directly on the wall before entering the central region. Therefore, for the discharge chamber in this study, the 2 MHz RF can achieve better performance than the 13.56 MHz frequency when the gas is xenon. Figure 8b shows the electron density distribution in the radius direction at the exit of the discharge chamber at the RF of 2 MHz. The electron density reaches the maximum at the center and decreases as it nears the wall. Meanwhile, the value of the beam current of the thruster can be estimated from the maximum value of the electron density at the exit of the discharge chamber, and the correctness of the numerical model can be

verified by comparing the test results. Equation 1 (Goebel and Katz 2008) expresses the relationship between the beam current and the screen grid ion density.

$$I_b = \frac{1}{2} n_i e v_a A_S T_S \tag{11}$$

where I_b is the beam current, n_i is the maximum value of ion density on the screen grid, v_a is the ion velocity, A_s is the screen grid area, and T_s is the effective transparency of the screen grid. The maximum value of the electron density at the exit of the discharge chamber obtained by Fig. 8b can be approximated as n_i, and the value of the beam current at different RF powers can be estimated as shown in Fig. 9.

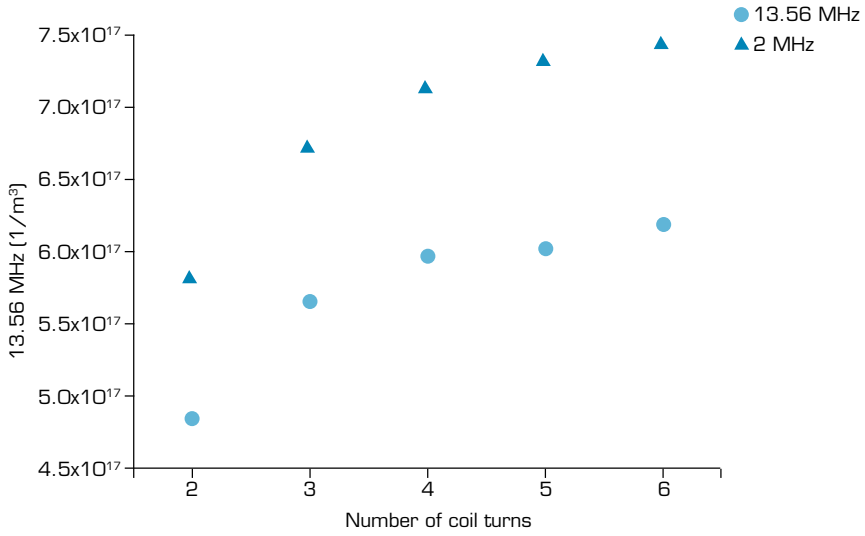

Figure 7. Electron density vs. number of coil turns at the axis of the discharge chamber with different operational frequency (2 and 13.56 MHz) electron density and temperature are the core plasma parameters that directly determine the macroscopic performance parameters of the thruster. To study their interaction laws, the distribution laws of electron density and temperature are calculated for different combinations of operational frequency and RF power at the same thruster geometry and the number of RF coil turns is six.

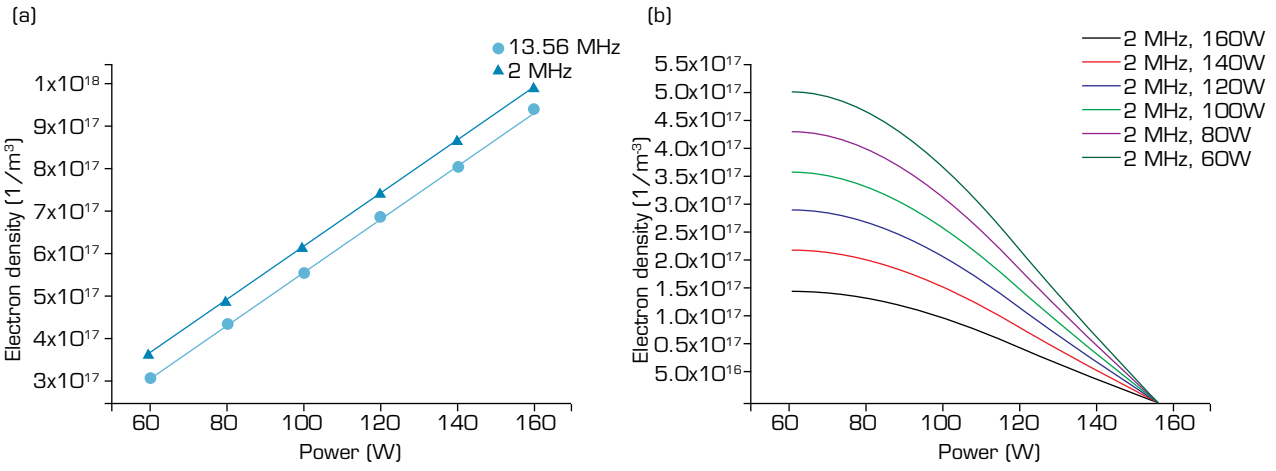

Figure 8. Electron density distribution at different RF power frequency and RF powers. (a) Electron density vs. RF power at the axis with different operational frequency (2 and 13.56 MHz); (b) Electron density distribution in the direction of the exit radius of the discharge chamber at different RF powers (2 MHz).

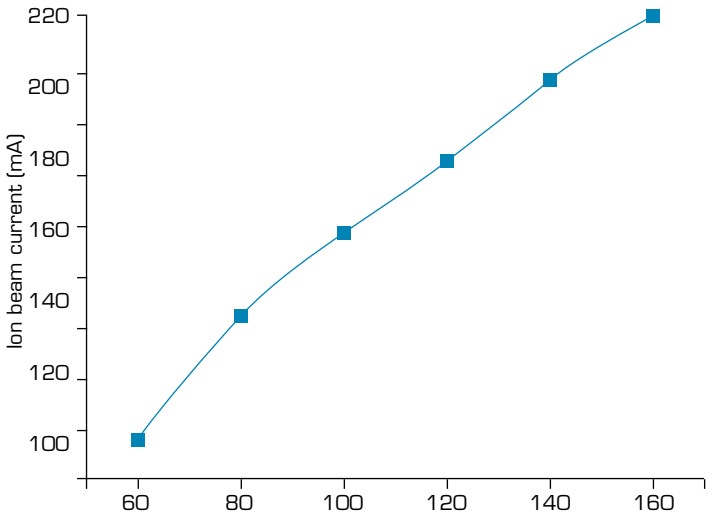

Figure 9. Simulation results of beam current vs. RF power.

Figure 10 shows the variation of the electron temperature with the RF power at different operational frequencies. The figure indicates that the electron temperature is basically unaffected by the operational frequency and RF power. Thus, the thruster beam flow can be regulated by adjusting the RF power while ensuring a low electron temperature range that does not severely corrode the gate wall material and affect the life of the thruster.

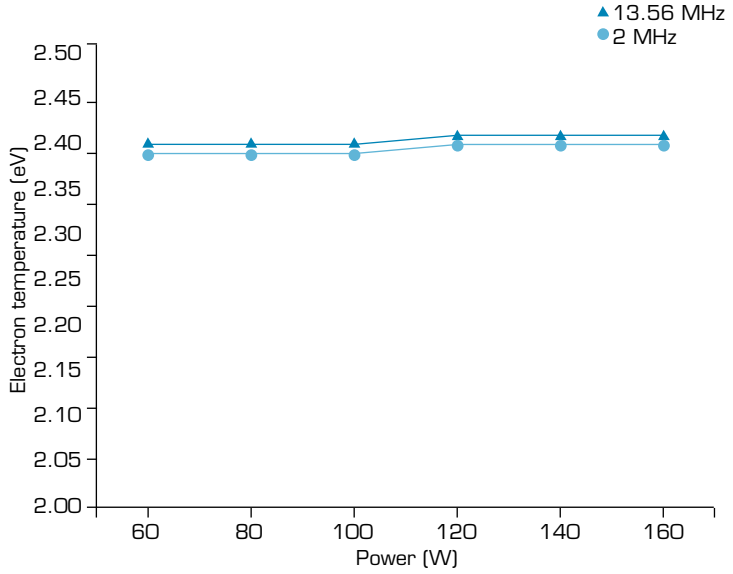

Figure 10. Electron temperature vs. RF power with different RF power frequencies.

THRUSTER AND TEST SECTIONS

The 10-cm DS4G RF ion thruster was used for the test. Figure 11 shows the structure and physical diagram of the thruster, which is mainly composed of a ceramic discharge chamber, RF coils, ion optic systems, gas distributor, gas path insulator, high voltage insulating ceramics, and other components.

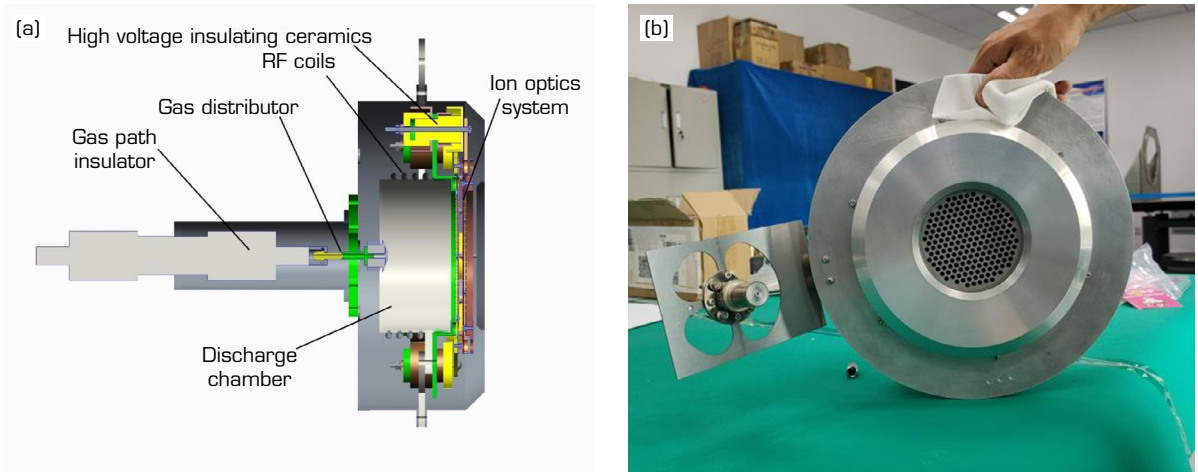

Figure 11. (a) Thruster construction; (b) Thruster physical drawing.

The cylindrical discharge chamber is the area where the plasma is generated and the core component of the thruster. Alumina ceramic was selected as the material for the discharge chamber of the thruster. According to previous simulations, the RF coil is wound six times on the outer wall of the discharge chamber.

Given the high screen grid voltage, the grid structure was optimized by reducing the screen grid opening area, increasing the screen grid thickness, and improving the voltage withstand capability. A 4-grid system consisting of 199 apertures, the active grid diameter is 80 mm and the thickness of grid is 1 mm. The specific geometric parameters are shown in Table 1.

Table 1. Geometrical parameters of the grid structure.

Parameters	Value
Grid diameter (mm)	100
Active grid diameter (mm)	80
Grid aperture number	199
Screen grid aperture diameter (mm)	5.0
Extraction grid aperture diameter (mm)	3.5
Acceleration grid aperture diameter (mm)	3.5
Deceleration grid aperture diameter (mm)	4.0
Screen grid thickness (mm)	1.0
Extraction grid thickness (mm)	1.0
Acceleration grid thickness (mm)	1.0
Deceleration grid thickness (mm)	1.0
Extraction stage gap (mm)	2.5
Acceleration stage gap (mm)	2.1
Deceleration stage gap (mm)	1.0

The 10-cm DS4G RF ion thruster validation test was carried out on the TS-6S electric propulsion performance test platform in the Lanzhou Institute of Physics, with a vacuum chamber diameter of 1.8 m, length of 4 m, background vacuum of 1×10^{-4} Pa, and operating vacuum of 8.2×10^{-4} Pa. The test system mainly consists of a RF ion thruster, a hollow cathode neutralizer, a ground-based RF power supply, a π-type RF matching network, a ground-based high-voltage power supply, a gas supply system, and parameter monitoring instruments, as shown in Fig. 12. The RF power supply is connected to the thruster coil via a π-type RF matching network, with an operational frequency of 2 MHz, a screen grid voltage of 4000 V, an extraction grid voltage of 2500 V,

an accelerating grid voltage of –200 V, a decelerating grid voltage of zero, a gas mass of xenon, a flow rate of 4 SCCM, a RF power of 0–500 W (continuously adjustable). Figure 13 is a photo of the beam generated by the thruster.

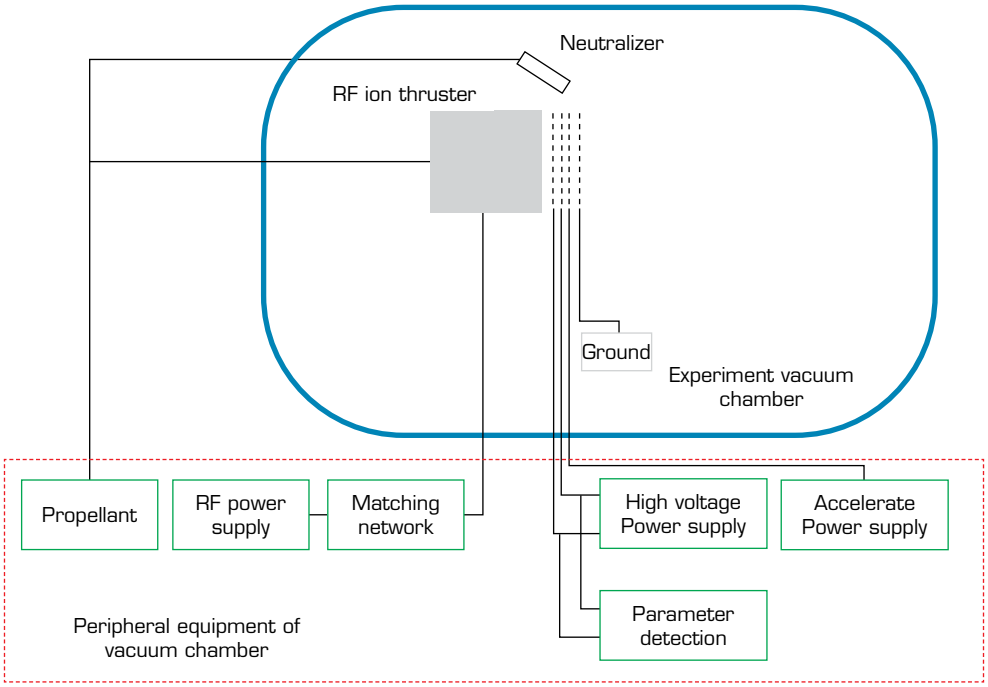

Figure 12. Thruster performance test system diagram.

Figure 13. Photo of beam generated by the thruster.

Thrust force F (mN), specific impulse I_{sp} (s), and mass utilization efficiency η (%) are usually used to characterize the performance of the thruster, and these parameters were not measured but calculated. The calculation formula is as follows (Eqs. 12–14):

$$F = \sqrt{\frac{2M}{e}} I_b \sqrt{V_b} \text{ [N]} \tag{12}$$

$$\eta = \frac{I_b}{eQ} \tag{13}$$

$$I_{sp} = \frac{\eta}{g} \sqrt{\frac{2eV_b}{M_a}} \tag{14}$$

where I_b is the screen grid current (beam current), V_b is the screen grid voltage (beam voltage), Q is the mass flow rate and M_a is the atomic mass. If the propellant is xenon, $\sqrt{2M/e} = 1.65 \times 10^{-3}$, M_a = 131.29. Equations 12–14 can be rewritten as:

$$F = 1.65 I_b \sqrt{V_b} \ \text{[mN]} \tag{15}$$

$$\eta = \frac{F}{72Q} \tag{16}$$

$$I_{sp} = 123.6 \eta \sqrt{V_b} \tag{17}$$

Screen grid voltage (V_b), mass flow rate (Q), and RF power (P_{RF}) are all provided as operating parameters, and the performance parameters of the thruster can be obtained by measuring the beam current, which is also commonly used to indirectly characterize the performance of the thruster.

Table 2 presents the summary of the 10-cm DS4G RF ion thruster performance. The thruster can achieve thrust of 10–23 mN, specific impulse of 2741–5970 s, and thruster density of 0.21–0.42 mN·cm^{-2} when the RF power varies within the range of 60–160 W. The experimental results show that the DS4G ion thruster with RF source can realize the super high specific impulse, and the maximum specific impulse of the thruster reaches 5930 s, which is nearly two times of the common ion thruster, as shown in Table 3 (Hu *et al.* 2020; Killinger *et al.* 2001; Thige *et al.* 2008). The improvement of the specific impulse of the thruster can effectively improve the utilization rate of the propellant. When the spacecraft is performing the same task, the use of the thruster with high specific impulse can effectively reduce the consumption of propellant, which will greatly improve the payload ratio of the spacecraft and provide the possibility for the spacecraft to realize farther deep space exploration.

Table 2. Summary of the 10-cm DS4G RF ion thruster performance.

Performance parameters	Value	Operating parameters	Value
Thruster (mN)	10–23	Beam potential (kV)	4
Specific impulse (s)	2741–5970	Extraction potential (kV)	2.5
Beam current (mA)	101–220	RF power (W)	60–160
Mass utilization efficiency (%)	35–76.4	Mass flow rate (SCCM)	4
Beam power (W)	400–880	Beam diameter (cm)	8
Thruster density (mN·cm^{-2})	0.21–0.42	Grid open area ratio (%)	77.7

Table 3. Specific impulse of the 10-cm DS4G RF ion thruster compared with the common ion thruster.

	DS4G	RIT-10	XIPS-8	LIPS-100
Specific impulse (s)	2741–5970	3400	2000–3000	175–3500
Beam diameter (cm)	8	8.7	8	10

To verify the accuracy of the numerical model, the RF power was adjusted (60–160 W) to obtain different beam current values. The comparison of the experimental and simulation results is shown in Fig. 14.

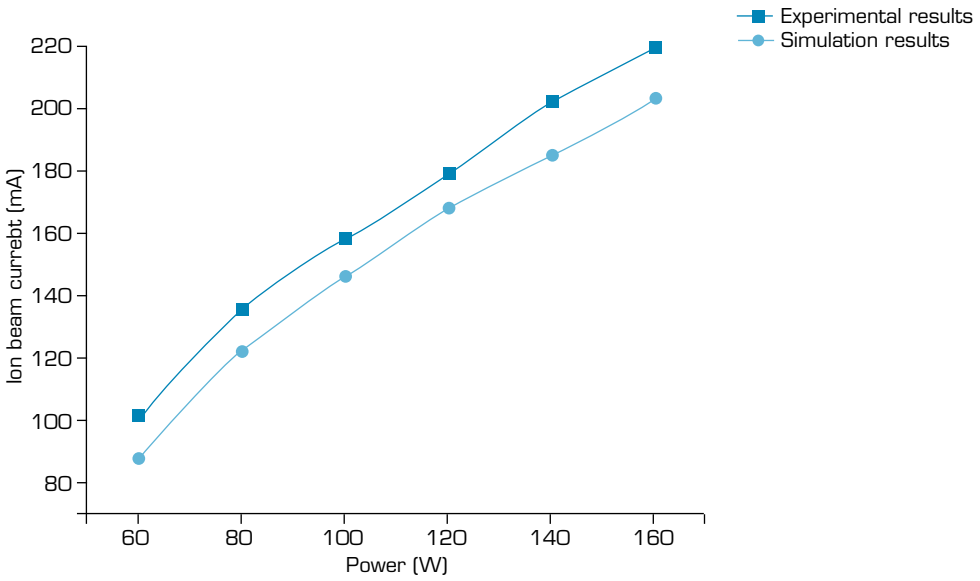

Figure 14. Comparison of test results and simulation result.

The results show that, as the RF power increases, the beam current values obtained from the simulation and the experimental test results show the same trend, that is, the beam current gradually increases as the RF power increases. Further comparison shows that the simulation results are smaller than the experimental results. Analysis suggests that the contribution of exchange-charged ions and neutral particles to the beam current is ignored in the simulation calculations, thus resulting in lower simulation results compared with the experimental results.

CONCLUSION

The simulation results show that increasing the number of RF coil turns can effectively improve the efficiency of inductive coupled discharge and reduce the energy dissipation generated by the coil. The operational frequency affects the characteristics of the inductively coupled discharge by influencing the depth of the plasma skinning layer. If the skinning layer is extremely small, then most of the energy will be deposited to the wall, and the ions generated in this region will directly compound with the wall, affecting the plasma density inside the discharge chamber. For the thruster in this study, 2 MHz of RF power is suitable. Increasing the RF power causes a linear increase in the electron density inside the discharge chamber without causing a significant increase in the electron temperature, which in turn allows the beam current to be regulated by adjusting the RF power while ensuring a low electron temperature. An experimental program implemented with a 10-cm DS4G RF ion thruster demonstrated the thruster can achieve super high specific impulse. In the experiment, a total beam potential of up to 4 kV was exhibited. The specific impulse reached 5970 s, the thrust reached 23 mN, and the maximum mass utilization efficiency reached 76.4%. Moreover, the correctness of the simulation model is also verified by the experimental results. Consequently, the numerical calculation model can provide support for the subsequent optimization of the DS4G RF ion thruster.

AUTHORS' CONTRIBUTION

Conceptualization: Pu Y and Li X; **Methodology:** Pu Y and Zhang W; **Investigation:** Jia L; **Writing-Original Draft:** Pu Y and Li X; **Writing – Review and Editing:** Pu Y and Liu X; **Funding Acquisition:** Sun X; **Resources:** WU C; **Supervision:** Wu X.

DATA AVAILABILITY STATEMENT

Data will be available upon request.

FUNDING

State Administration of Science, Technology and Industry for National Defense of China
Grant No: JCKY2018203B030

National Natural Science Foundation of China
[https://doi.org/10.13039/501100001809]
Grant No. 61801201

Science and Technology Plan of Gansu Province of China
Grant No. 18JR3RA412

Outstanding Youth Fund of Gansu Province of China
Grant No. 20JR10RA481

ACKNOWLEDGEMENTS

The authors are thankful to the Science and Technology on Vacuum Technology and Physics Laboratory for providing the test data.

REFERENCES

Bramanti C, Walker R, Sutherland O, Boswell R, Charles C, Fearn D, Del Amo JG, Orlandi M (2006) The innovative dual-stage 4-grid ion thruster concept: Theory and experimental results. Paper presented 57th International Astronautical Congress. AIAA; Valencia, Spain. https://doi.org/10.2514/6.IAC-06-C4.4.07

Chabert P, Monreal JA, Bredin J, Popelier L, Aanesland A (2012) Global model of a gridded-ion thruster powered by a radiofrequency inductive coil. Phys Plasmas 19:73512-73519. https://doi.org/10.1063/1.4737114

El-Fayoumi IM, Jones IR (1998) The electromagnetic basis of the transformer model for an inductively coupled RF plasma source. Plasma Sources Sci Technol 7(2):179-185. https://doi.org/10.1088/0963-0252/7/2/012

Goebel DM (2008) Analytical discharge model for RF ion thruster. IEEE Trans Plasma Sci 36(5):2111-2121. https://doi.org/10.1109/TPS.2008.2004232

Goebel DM, Katz I (2008) Fundamentals of electric propulsion: Ion and hall thrusters. Hoboken: John Wiley & Sons. https://doi.org/10.1002/9780470436448

Henrich R, Heiliger C (2013) Three dimensional simulation of micro Newton RITs. Paper presented 33rd International Electric Propulsion Conference. IEPC; Washington DC, United States of America. [accessed Mar 5 2021]. http://electricrocket.org/IEPC/ixkapkx1.pdf

Hu J, Yang F, Guo D, Gu Z, Shao M, Zheng M (2020) [Research on variable thrust characteristics of 10-cm xenon ion thruster]. [Propulsion Technology] 41(10):2382-2389. Chinese. https://doi.org/10.13675/j.cnki.tjjs.190562

Keller JH, Foster JC, Barnes MS (1993) Novel radio-frequency induction plasma processing techniques. J Vac Sci Technol A 11:2487-2491. https://doi.org/10.1116/1.578597

Lucken R, Marmuse F, Bourdon A, Chabert P, Tavant A (2019) Global model of a magnetized ion thruster with xenon and iodine. Paper presented 36th International Electric Propulsion Conference. IEPC; Vienna, Austria. [accessed Mar 5 2021]. http://electricrocket.org/2019/678.pdf

Mazouffre S (2016) Electric propulsion for satellites and spacecraft: Established technologies and novel approaches. Plasma Sources Sci Technol 25(3):033002. https://doi.org/10.1088/0963-0252/25/3/033002

Pham QTD, Shin J (2020) Better prediction of the performance of a radio-frequency ion thruster. J Korean Phys Soc 76: 137-144. https://doi.org/10.3938/jkps.76.137

Piejak RB, Godyak VA, Alexandrovich BM (1992) A simple analysis of an inductive RF discharge. Plasma Sources Sci Technol 1(3):179-186. https://doi.org/10.1088/0963-0252/1/3/006

Killinger R, Bassner H, Kukies R, Leiter H (2001) Result of the 15000 hours lifetime test for the RITA ion propulsion on ESA'S ARTEMIS satellite. Paper presented 27th International Electric Propulsion Conference. IEPC; Pasadena, California, United States of America. [accessed Mar 8 2021]. http://electricrocket.org/IEPC/82_1.pdf

Rakhimov RG, Kharlan YY, Uzhinsky I, Milov AE, Aypov RE, Cherniy IA (2019) Numerical simulation of plasma discharge in RF ion thruster. Paper presented 36h International Electric Propulsion Conference. IEPC; Vienna, Austria. [accessed Mar 8 2021]. http://electricrocket.org/2019/496.pdf

Takahashi K, Akahoshi H, Charles C, Boswell RW, Ando A (2017) High temperature electrons exhausted from rf plasma sources along a magnetic nozzle. Phys Plasmas 24(8):084503. https://doi.org/10.1063/1.4990110

Tsay M, Martinez-Sanchez M (2008) Two-dimensional simulation of a radio-frequency ion thruster discharge. Paper presented 44nd AIAA/ASME/SAE/ASEE Joint Propulsion Conference & Exhibit. AIAA; Hartford, Connecticut, United States of America. https://doi.org/10.2514/6.2008-5196

Thige W, Chien K-R, Ahn J, Hurtado J, Solis E, Spears R (2008) Update on the XIPS 8-cm thruster prototype. Paper presented 44th AIAA/ASME/SAE/ASEE Joint Propulsion Conference & Exhibit. AIAA; Hartford, Connecticut, United States of America. https://doi.org/10.2514/6.2008-4912